J. Fluid Mech. (1989), *vol.* 201, *pp.* 485–505
Printed in Great Britain

Unsteady separated wake behind an impulsively started cylinder in slightly viscous fluid

By A. Y. CHEER
Department of Mathematics, University of California, Davis, CA 95616, USA

(Received 27 January 1984 and in revised form 16 September 1988)

The initial unsteady two-dimensional flow around an impulsively started circular cylinder is investigated using the random-vortex numerical method. To understand the mechanisms of the primary and secondary vortex formation, we investigate the relationship between the creation, diffusion and convection of vorticity to the genesis and evolution of the complex and 'unstable' flow structures of the recirculating zone behind the cylinder. Our simulation reveals detailed geometric features of the wake which are in agreement with experimental observations and with other numerical calculations. Numerical calculation at Reynolds numbers $R = 3000$, 9500 and 10^4 show that the numerical method is appropriately sensitive to changes of the Reynolds number. Numerical functionals such as the length of the wake, velocity on the wake axis and the angle of separation for our calculations are in satisfactory agreement with known experimental and numerical results. This numerical method gives results comparable to those of a previously published method but does so using much less memory and computer time.

1. Introduction

It is generally recognized that one of the most important unexplained phenomena concerning flows past obstacles at high Reynolds numbers is the development of the unsteady wake. A fundamental understanding of the behaviour of unsteady flows has significant implications for the solution of many fluid dynamic problems. Nevertheless, the challenges in studying unsteady flow are considerable. Not only are the equations involved nonlinear and the viscosity small, but the development of the wake is extremely complex owing in part to the instability of some of the recirculating structures. Moreover, the Navier–Stokes equations, which describe viscous fluid flows, are so complicated that analytical and numerical treatments, especially at large Reynolds numbers, are very difficult. The analytic solution to these equations, as with most nonlinear partial differential equations, has eluded theoretical analysis except for a few very special cases. On the other hand, attempts to utilize numerical methods face several important constraints. For example, in the study of unsteady flow of an incompressible fluid past an object at high Reynolds numbers, R, the crucial region is small in size and, in addition, involves boundaries and vortex sheets. This puts the numerical method based on a grid at a considerable disadvantage because the mesh width must decrease as R increases. Consequently, at very large R, a very fine grid must be imposed or else the numerical viscosity due to the grid will swamp the effects of the true viscosity as represented by the Reynolds number.

There have been a plethora of numerical studies analysing separated flow around an impulsively started circular cylinder. Payne (1958) was one of the first to use a

finite-difference method to simulate unsteady symmetric viscous flow past an impulsively started cylinder for $R = 40$ and 100. Similar methods have been subsequently used by many authors including Ingham (1968), Son & Hanratty (1969), Thoman & Szewczyk (1969), Dennis & Staniforth (1971), Telionis & Tsahalis (1974) and Lin, Pepper & Lee (1975). More recently investigators like Ta Phuoc Loc (1980) used second- and fourth-order compact finite-difference schemes to study unsteady flow at $R = 300$, 500 and 1000. Lecointe & Piquet (1984) used a second- and fourth-order accurate method of mehrstellen type to study flow at $R = 200$ to 3000, and Rogers, Kwak & Kual (1985) used a pseudocompressibility method to study the symmetric wake at $R = 1200$. Until recently, most of the numerical calculations diverged from experimental data at around $R = 1200$. Lecointe & Piquet showed the development of the secondary vortices at $R = 3000$, but the resolution of their calculations is not good. Cheer (1983*b*) was able to reproduce the secondary vortex structures at $R = 9500$ using a vortex method, and Ta Phuoc Loc & Bouard (1985) later extended their difference scheme to a flow at $R = 3000$ and 9500. Finite-element methods and spectral methods have also been successfully used (see Shen 1977; Gottlieb & Orszag 1977; Peyret & Taylor 1983).

Experimentalists working to understand the phenomena of unsteady wake formation have been able to visualize flow past impulsively started circular cylinders for various Reynolds numbers. Using the aluminium powder method Honji & Teneda (1969) studied flows at $R = 40$–1700, Coutanceau & Bouard (1977, 1979) and Bouard & Coutanceau (1980) produced flow visualizations for $R = 40$–9500 by reflecting magnesium or diffusing rilsan solid tracers, and Nagata, Funada & Matsui (1985*b*), and Nagata *et al.* (1985*a*) used a combination of the aluminium dust and the hydrogen bubble technique to study flow at $R = 1200$. Among the various aspects of the development of the unsteady wake studied by these investigators are functionals such as the size of the pair of standing eddies formed behind the cylinder, the separation angle measured as a function of time and the timing of the delicately formed secondary vortices. Nagata *et al.* (1985*a*) also attempted to study the process of vorticity transfer by analysing the combination of the velocity field and the streamlines.

In this paper, we examine the mechanism of the creation of the primary and secondary vortex structures behind an impulsively started circular cylinder at Reynolds numbers 3000–10^4. The process of vortex and secondary vortex formation can be regarded as a process of vorticity transfer – that is, the creation of vorticity on the boundary due to the no-slip boundary condition, the diffusion of the vorticity from the boundary, the convection of the vorticity produced on the surface of the cylinder through the separation point and the redistribution of the vorticity behind the cylinder resulting in primary and secondary vortex formation. This time-dependent process of vorticity creation, diffusion and convection is reproduced in the numerical algorithm by tracking the creation and motions of computational vortex elements, which carry concentrations of vorticity (sheet elements) or circulation (blob elements). The velocity field is reconstructed from the position and concentration of vorticity or circulation of these computational elements.

2. The numerical method

Consider the two-dimensional Navier–Stokes equations in vorticity formulation in the absence of any boundaries. We denote $\boldsymbol{u} = (u, v)$ to be the velocity vector,

$z = (x, y)$ the position vector, $\xi = \text{curl}\,(u, v)$ the vorticity, ψ the stream function, R the Reynolds number and ∇^2 the Laplacian.

$$\xi_t + (\boldsymbol{u} \cdot \nabla)\,\xi = R^{-1}\nabla^2\xi, \tag{1a}$$

$$\nabla^2\psi = -\xi, \tag{1b}$$

$$u = \psi_y, \quad v = -\psi_x. \tag{1c}$$

We split the above system of equations up into two parts: an inviscid and a viscous part

$$\xi_t + (\boldsymbol{u} \cdot \nabla)\,\xi = 0, \tag{2a}$$

$$\nabla^2\psi = -\xi, \tag{2b}$$

$$u = \psi_y, \quad v = -\psi_x; \tag{2c}$$

$$\xi_t = R^{-1}\nabla^2\xi, \tag{3a}$$

$$\xi = \xi(z, t). \tag{3b}$$

The inviscid (Euler) equations are modelled using the vortex-blobs method and the diffusion equation is modelled using random walks. This method, presented by Chorin (1973), is a grid-free numerical method where the nonlinear terms of the equations are studied through inviscid interactions between vortex blobs of small compact support, and the effects of viscosity are studied through use of the relationship between diffusion and random walks.

At any time $t > 0$, the vortex elements already in the flow will move according to the discrete approximation to Euler's equations $(2a, b, c)$

$$x_i^{n+1} = x_i^n + \Delta t\, u_i^n, \tag{4a}$$

$$y_i^{n+1} = y_i^n + \Delta t\, v_i^n, \tag{4b}$$

where

$$u_i^n = -\frac{1}{2\pi}\sum_{r_{ij}>\sigma} k_j \frac{y_i^n - y_j^n}{r_{ij}^2} - \frac{1}{2\pi}\sum_{r_{ij}\leqslant\sigma} k_j \frac{y_i^n - y_j^n}{\sigma r_{ij}}, \tag{5a}$$

$$v_i^n = +\frac{1}{2\pi}\sum_{r_{ij}>\sigma} k_j \frac{x_i^n - x_j^n}{r_{ij}^2} + \frac{1}{2\pi}\sum_{r_{ij}\leqslant\sigma} k_j \frac{x_i^n - x_j^n}{\sigma r_{ij}}, \tag{5b}$$

and where Δt is the time step, (x_i^n, y_i^n) is the position of the ith vortex element at time $t = n\,\Delta t$,

$$r_{ij} = [(x_i^n - x_j^n)^2 + (y_i^n - y_j^n)^2]^{\frac{1}{2}}, \quad r_{ij}^2 = (x_i^n - x_j^n)^2 + (y_i^n - y_j^n)^2,$$

σ is the cutoff value, and k_j is the strength of the vortex-blob element whose centre is (x_j^n, y_j^n).

Convergence proofs for this numerical method are given by Hald & Del Prete (1978), Hald (1979, 1985) and Beale & Majda (1982a, b). The rate of convergence depends in part on how σ is chosen and how well the velocity (u, v) is approximated. In the calculations for this paper, σ is chosen to be h/π for a specific reason to be discussed later, and a second-order-accurate predictor–corrector algorithm is used to obtain the (u, v) velocities.

Viscosity is included in the algorithm by adding a random-walk component to the

discrete solution of Euler's equations above. Random walks are used to approximate the solution to the diffusion equations $(3a, b)$. Thus the discrete approximations to $(1a, b, c)$ are

$$x_i^{n+1} = x_i^n + \Delta t\, u_i^n + \eta_i^1, \tag{6a}$$

$$y_i^{n+1} = y_i^n + \Delta t\, v_i^n + \eta_i^2, \tag{6b}$$

where η_i^1, η_i^2 are independent random variables with a Gaussian distribution of mean zero and variance $2\Delta t/R$.

Roberts (1983) computationally tested the accuracy of the random-vortex method and confirmed the error to be $O(1/N^{\frac{1}{2}}R)$, where N is the number of computational elements. Marchioro & Pulvirenti (1982) demonstrated analytically that the random-vortex construction represents a weak solution to the Navier–Stokes equations. Goodman (1986) extended work in this direction by giving a convergence proof of the method. He showed that (with high probability) this method will produce good approximations to the true velocities. Moreover, with sufficient smoothing, there are no serious restrictions on the time step Δt; as long as Δt goes to zero as N goes to ∞ and $\Delta t \geqslant CN^{-p}$ for some $p > 0$, the method will converge. Beale & Majda (1981), and Anderson & Greengard (1985) also have discussed errors introduced in the viscous splitting, in the approximate solution to the inviscid Euler's equations, in the smoothing and in sampling.

When we introduce an object into the flow, which in our case is a circular cylinder, we need to satisfy the no-slip boundary conditions:

$$\boldsymbol{u} \cdot \boldsymbol{n} = 0 \quad \text{on the boundary } \partial D, \qquad \boldsymbol{n} \quad \text{normal to } \partial D, \tag{7a}$$

$$\boldsymbol{u} \cdot \boldsymbol{\tau} = 0 \quad \text{on the boundary } \partial D, \qquad \boldsymbol{\tau} \quad \text{tangent to } \partial D. \tag{7b}$$

To satisfy the normal boundary conditions, we use the method of images for the vortex blobs, and to satisfy the tangential boundary conditions, a vorticity generation algorithm is used.

In order to improve convergence on the boundary of the object, vortex-sheet elements instead of vortex-blob elements are created as a result of the no-slip boundary condition by the numerical algorithm. These vortex-sheet elements diffuse away from the boundary and are convected downstream, producing a layer of large vorticity adjacent to the solid surface. Through this boundary layer the tangential velocity falls from its value in the main stream to zero at the solid surface. The vortex-sheet elements move and diffuse according to the boundary-layer equations:

$$\xi_t + (\boldsymbol{u} \cdot \boldsymbol{\nabla})\, \xi = R^{-1} \xi_{yy}, \tag{8}$$

$$\xi = -u_y, \tag{9}$$

$$u_x + u_y = 0, \tag{10}$$

with boundary conditions

$$\boldsymbol{u} = (u, v) = (0, 0) \quad \text{at} \quad y = 0, \tag{11a}$$

$$u(x, y = \infty) = U_\infty(x). \tag{11b}$$

In this set of equations, u refers to the velocity component in the tangential direction and v is the velocity component in the direction normal to the boundary. Similarly (x, y) refers to the position in (θ, r) coordinates.

To approximate this set of equations numerically, we once again split the operator into an inviscid and a viscous part:

$$\xi_t + (\boldsymbol{u} \cdot \nabla)\xi = 0, \tag{12a}$$

$$\xi = -u_y, \tag{12b}$$

$$u_x + u_y = 0; \tag{12c}$$

$$\xi_t = R^{-1}\xi_{yy}, \tag{13a}$$

$$\xi_0 = \xi(x, y, t = 0). \tag{13b}$$

The inviscid part of the equations is modelled using vortex-sheet elements and the viscous part is modelled using random walks. This method was introduced by Chorin in 1978. See Chorin (1978, 1980) for more details. For a documentation of a computer program implementing the vortex-sheets method for the boundary-layer equations see Cheer (1978).

The vortex sheets move according to the discrete approximation to equations (12*a*, *b*, *c*):

$$x_i^{n+1} = x_i^n + \Delta t\, u_i^n, \tag{14a}$$

$$y_i^{n+1} = y_i^n + \Delta t\, v_i^n, \tag{14b}$$

where $$u_i^n = U_\infty(x_i^n) - \tfrac{1}{2}\xi_i - \sum_j \xi_j d_j, \qquad d_j = 1 - |x_i^n - x_j^n|\, h^{-1},$$

Σ_j is the sum over all vortex sheets s_j such that $y_j^n > y_i^n$, h is the length of the sheet,

$$v_i^n = \frac{-(I_1 - I_2)}{h},$$

$$I_1 \approx U_\infty(x_i^n + \tfrac{1}{2}h)\, y_i^n - \sum_j \xi_j d_j^+ y_j^{*n},$$

$$I_2 \approx U_\infty(x_i^n + \tfrac{1}{2}h)\, y_i^n - \sum_j \xi_j d_j^- y_j^{*n},$$

$$d_j^+ = 1 - \frac{|(x_i^n + \tfrac{1}{2}h) - x_j^n|}{h}, \qquad d_j^- = 1 - \frac{|(x_i^n - \tfrac{1}{2}h) - x_j^n|}{h},$$

$$y_j^{*n} = \min(y_i^n, y_j^n),$$

Σ_+ is the sum over all vortex sheets S_j such that $0 \leqslant d_j^+ \leqslant 1$, and Σ_- is the sum over all vortex sheets S_j such that $0 \leqslant d_j^- \leqslant 1$.

For the present study, a second-order predictor–corrector scheme for the calculation of the velocities (u, v) is used. Once again, the effects of viscosity are included by adding to the normal component of the solution an independent random variable η_i drawn from a Gaussian distribution of mean zero and variance $2\Delta t/R$. Thus

$$x_i^{n+1} = x_i^n + \Delta t\, u_i^n, \tag{15a}$$

$$y_i^{n+1} = y_i^n + \Delta t\, v_i^n + \eta_i. \tag{15b}$$

Convergence results for the vortex-sheet method are given by Puckett (1987). He also performed numerical experiments varying the numerical parameters and claimed that, unlike the vortex-blobs method, the added accuracy introduced by using a higher-order approximation for the velocities (u, v) is swamped, over time, by the errors in the random-walk solution. He proved that for $\Delta t = O(N^{-\frac{1}{4}})$ the numerical

method converges like $\ln N(N^{-\frac{1}{4}})$ uniformly as the diffusion coefficient $(1/R)$ tends to 0.

These two methods are coupled at the edge of the boundary layer. By choosing the cutoff $\sigma = h/\pi$, it can be shown that the velocity induced on the boundary by a blob is identical to the velocity induced by a sheet sitting at the same point at the edge of the boundary (see Cheer 1983*a*). Thus, as a vortex sheet leaves the boundary layer and becomes a vortex blob, its effect on the boundary condition is the same.

To satisfy the normal boundary condition, we use the method of images on the vortex blobs. The resulting u- and v-velocities satisfying $\boldsymbol{u} \cdot \boldsymbol{n} = 0$ are

$$u_i = 1 - \frac{(x_i^2 - y_i^2)}{(r_i^2)^2} + \frac{1}{2\pi}\sum_j k_j \frac{y_i - y_j}{(r_{ij})^2} + \frac{1}{2\pi}\sum_j k_j \frac{(y_i - y_j)}{\sigma(r_{ij})}$$

$$- \frac{1}{2\pi}\sum_j k_j \frac{(y_i - y_j/r_j^2)}{(r_{ij}^*)^2} - \frac{1}{2\pi}\sum_j k_j \frac{(y_i - y_j/r_j^2)}{\sigma(r_{ij}^*)}, \tag{16a}$$

$$v_i = -\frac{2x_i y_i}{(r_i^2)^2} - \frac{1}{2\pi}\sum_j k_j \frac{x_i - x_j}{(r_{ij})^2} - \frac{1}{2\pi}\sum_j k_j \frac{(x_i - x_j)}{\sigma(r_{ij})}$$

$$+ \frac{1}{2\pi}\sum_j k_j \frac{(x_i - x_j/r_j^2)}{(r_{ij}^*)^2} + \frac{1}{2\pi}\sum_j k_j \frac{(x_i - x_j/r_j^2)}{\sigma(r_{ij}^*)}, \tag{16b}$$

where

$$r_i = (x_i^2 + y_i^2)^{\frac{1}{2}}, \qquad (r_i)^2 = (x_i^2 + y_i^2),$$

$$r_{ij} = [(x_i - x_j)^2 + (y_i - y_j)^2]^{\frac{1}{2}},$$

$$r_{ij}^* = \left[\left(x_i - \frac{x_j}{r_j^2}\right)^2 + \left(y_i - \frac{y_j}{r_j^2}\right)^2\right]^{\frac{1}{2}},$$

$$(r_j)^2 = x_j^2 + y_j^2, \qquad \sigma = h/\pi,$$

Σ_1 is taken over all vortices such that $r_i, r_{ij}, r_{ij}^* > \sigma$, and Σ_2 is taken over all vortices such that $r_i, r_{ij}, r_{ij}^* < \sigma$.

Developments, modifications, discussions, extensions and applications of the random-vortex method to a variety of flow problems are reviewed in Leonard (1980), Aref (1983) and Ghoneim & Sherman (1985).

3. Problem statement and numerical parameters

Initially, at time $t = 0$, the cylinder of radius one is assumed to be at rest in a stationary fluid of density $\rho = 1$. At some instant in time $t > 0$, the cylinder is set into motion impulsively with some uniform and constant translational velocity U_∞. We consider the flow development in a two-dimensional cross-section (see figure 1).

The numerical parameters used in this study are as follows. The circular cylinder of radius 1 is divided into equal pieces each of arclength $h = \pi/M$, where M varies from 20 to 50. The maximum strength allowable for each vortex sheet is $\xi_{\max}$ ($\xi_{\max}$ varies between 0.25 and 0.5) and the maximum circulation for the vortex points is $h\xi_{\max}$. For $M = 20$ and $\xi_{\max} = 0.25$, $h\xi_{\max} = 0.0785$. The Reynolds number $R = (\rho U_\infty D/\nu)$ where ρ = density = 1, U_∞ = free-stream velocity = 1, D = diameter of the cylinder and ν = viscosity. The time step Δt varies from $\Delta t^* = 0.03$ to 0.005, where $t = t^* U_\infty/D$. These choices for the above parameters are consistent with theoretical results and with the results presented in Sethian & Ghoniem (1986) who studied the

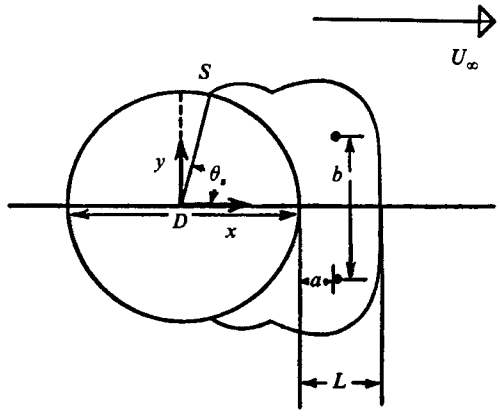

FIGURE 1. S refers to the point of separation, θ_s is the angle of separation, D is the diameter of the cylinder, L is the length of the wake and (a, b) is the location of the centre of the main vortex.

effect of variation of nearly all possible numerical parameters on the accuracy of the solution generated by the random-vortex method.

In the present study, for $R = 10^4$ and 9500 the flow is simulated from impulsive start to two diameter movements of the cylinder, and from impulsive start to three diameter movements for $R = 3000$. To allow comparison of our results to experimental data and other numerical calculations, symmetry with respect to the x-axis is imposed by reflecting the vortex elements in the upper half plane to the lower half plane. This is justifiable since the flow is known to be symmetric in the initial stages of development (see Bouard & Coutanceau 1980, and Batchelor 1967, Plate 10).

For the case $M = 20$, $\xi_{\max} = 0.25$, $h\xi_{\max} = 0.0785$, $R = 9500$ and $\Delta t^* = 0.03$, we start out with 112 computational elements and end up with 906 after two diameter movements of the cylinder. This simulation took about 15 minutes of CPU time on a Celerity mini-computer, and required less than 5000 words of computer memory. In contrast, Ta Phuoc Loc & Bouard's (1985) difference calculations used a grid of size 101×141, or 14000 locations where the solution must be determined before advancing to the next time step for $R = 3000$, and a grid of up to 101×301 for $R = 9500$. Such a large computational grid requires the storage and computational time of a supercomputer. For problems involving an incompressible fluid, the effects at infinity must be calculated correctly. In a difference scheme the grid must be sufficiently large in order to incorporate this condition accurately. Moreover in using higher-order approximation schemes one needs to be careful that oscillations based on the numerical scheme are not introduced into the solution. The vortex method incorporates this condition at infinity via the Biot–Savart Law (see Chorin 1973 and Leonard 1980).

4. Results

4.1. *Circulation and vorticity distribution*

In order to understand the mechanism of the development of secondary vortices and the mechanisms of vorticity transfer, we look at the time variation of vorticity creation on the boundary and distribution of circulation around the cylinder. This is done by tracking the motion of the vortex elements used to simulate the flow.

Angle\t^*	0.50	0.75	1.00	1.25	1.50	2.00
1.80	0.06	0.05	0.62	0.06	0.06	0.06
9.00	0.16	0.12	0.19	0.22	0.13	0.15
16.20	0.36	0.26	0.54	0.51	0.31	0.26
23.40	0.67	0.73	0.57	0.68	0.50	0.70
30.60	0.42	0.63	0.95	0.89	0.70	0.72
37.80	0.90	0.59	0.82	0.79	0.27	0.77
45.00	1.09	0.12	1.31	1.04	0.52	0.36
52.20	1.23	0.85	1.12	1.36	1.02	1.00
59.40	1.35	1.31	1.39	1.11	0.14	1.13
66.60	1.31	0.69	1.11	0.83	0.03	0.04
73.80	0.69	0.73	1.71	1.00	0.67	0.54
81.00	0.24	0.98	1.01	0.45	0.00	−0.45
88.20	1.09	0.09	1.33	−0.52	−0.35	−0.56
95.40	0.25	−0.29	1.13	−0.05	−0.87	−0.62
102.60	0.24	−0.28	1.17	−0.15	−0.29	−0.38
109.80	0.40	−1.25	−0.14	−0.60	−0.14	−0.68
117.00	−0.36	−2.32	−0.22	0.22	0.67	−0.55
124.00	−0.55	−1.70	0.85	1.75	−1.71	0.63
131.40	−0.74	−0.98	−1.62	−0.79	−0.41	0.72
138.60	−0.13	−0.96	−2.01	−1.33	−1.02	−1.36
145.80	−0.66	−0.62	−1.20	−1.77	−1.27	−0.77
153.00	0.01	−0.72	−0.92	−1.28	−1.18	−0.70
160.20	−0.43	−0.89	−0.28	−1.12	−1.15	−0.87
167.40	0.12	−0.14	−0.49	−0.36	−0.65	−0.47
174.60	−0.22	−0.34	−0.19	−0.19	−0.17	−0.15

TABLE 1. Time variation of the boundary condition. The values in the columns indicate the amount of vorticity to be created by the vorticity-creation algorithm in the portion of the cylinder that is below the x-axis. Zero degrees correspond to the front stagnation point and 180 degrees correspond to the rear stagnation point.

At time $t^* = 0$, the flow is potential. Immediately after impulsive start, vortex-sheet elements are generated on the boundary of the cylinder to satisfy the tangential boundary conditions. The sign of the vorticity created is negative in the upper half of the cylinder and positive in the lower half. For the numerical parameters, $M = 20$, $\xi_{\max} = 0.25$, $\Delta t^* = 0.03$ and $R = 9500$, 112 vortex-sheet elements are created initially to satisfy the tangential boundary conditions. These sheet elements move along the boundary towards the rear of the cylinder by convection and diffuse away from the cylinder by random walks. This process will uncover sections of the cylinder where more vortex sheets need to be created in order to satisfy the tangential boundary conditions. Table 1 gives the time variation of this boundary condition around the bottom half of the cylinder for one numerical experiment. Some of the sheets in the boundary layer will move into the outer flow where they are turned into vortex blobs. From time $t^* = 0.05$ to 0.75, there are, on average, about twice as many sheets created at each time step to satisfy the tangential boundary condition as there are sheets leaving the boundary layer and becoming blobs. The circulation per unit area around the cylinder is calculated in the following way. The cylinder is divided into 50 equal pieces, each of arclength $\pi/50$ and width 0.05. Vortex elements whose centres lie within an area are summed and divided by the area. The results are given in table 2. The results show that a peak in circulation occurs around time $t^* = 0.75$. Numerical calculations of Van Dommelen & Shen (1982) reveal a singularity in the

Angle\t^*	0.50	0.75	1.00	1.25	1.50	2.00
3.60	0	0	0	0	0	0
18.00	10.72	24.11	9.62	5.85	23.29	20.67
32.40	45.16	27.26	25.26	28.75	24.95	32.35
46.80	45.25	139.72	29.00	33.37	66.80	119.10
61.20	97.97	82.83	55.84	66.36	113.13	101.64
75.60	97.47	65.63	60.58	58.34	87.84	81.80
90.00	83.93	112.66	59.04	174.50	88.53	157.23
104.40	93.69	197.44	102.37	38.04	−16.49	61.77
118.80	72.15	38.51	19.05	−12.49	−71.34	−14.32
133.20	140.60	27.81	−24.20	−50.30	−68.68	−55.58
147.60	77.64	2.61	−16.07	−31.81	−53.77	−58.71
162.00	53.55	5.17	15.40	2.68	−21.23	1.19
176.40	18.26	8.33	−6.13	−12.19	0.00	0.00

TABLE 2. The half circle below the x-axis is divided into 25 pieces each of arc-length $\pi/25$. The average of the circulation in each of the pieces that is between the cylinder and 0.05 distance from the cylinder is calculated. Values in every other grid is presented above. Zero degrees correspond to the forward and 180 degrees correspond to the rear stagnation point.

boundary-layer solution at about $t^* = 0.75$ corresponding to vortex peeling and separation. Ta Phuoc Loc & Bouard exhibit a peak in vorticity in their numerical solution. Another peak in circulation appears around time $t^* = 1.25$.

In contrast to the early development of the flow (from impulsive start to $t^* = 0.75$), in the time interval from $t^* = 0.75$ to 2.00, the number of vortex sheets created on the boundary equals, on average, the number of sheets that leave the boundary layer and turn into blobs. Some of the vortex elements produced on the surface accumulate temporarily near the separation point and form a secondary vortex region. The incorporation of vortex elements into the main eddy is a combination of the vortex elements leaving through the point of separation and the shedding of secondary vortices.

At time $t^* = 2.00$, there are a total of $N = 906$ computational elements representing the flow: one half above and one half below the axis of symmetry. Of these 906 elements, 290 are vortex sheets and 616 are vortex blobs.

4.2. *Development of the vortex structures in the recirculating zones*

Figures 2–8 are computer graphs of the velocity vector field behind the circular cylinder at different times of the flow development at $R = 9500$ and 10^4. Many detailed results have been deleted in view of their general similarity to those presented by Ta Phuoc Loc & Bouard (1985) in a paper submitted later but published earlier. The length of the vectors in the figures corresponds to the speed of the fluid at that point, and the arrow indicates the direction of the flow. Arrowheads without tails indicate that the velocity is very small there. The first coherent 'vortex' structure appears at time $t^* = 0.75$ (see figure 2). At time $t^* = 1.00$, a complex flow pattern emerges (see figures 3, 4). The streamline plot shows that there are three distinct regions. The largest of these regions comprises the main vortex – the same one seen originally at $t^* = 0.75$. The velocity of the flow in this vortex is quite strong and the centre of the vortex has migrated downstream. The second region is a recirculating zone below the main vortex. This recirculating structure contains little vorticity (see figure 3*b*). The third region is a region of high

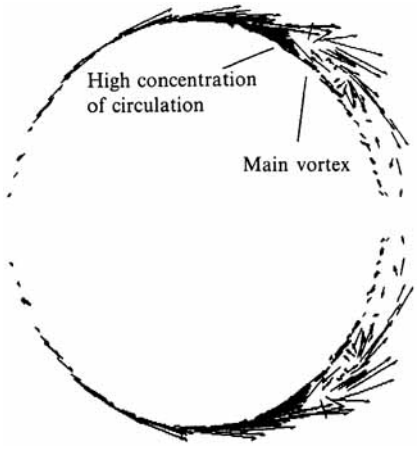

FIGURE 2. Plot of the induced velocity of each vortex element in the flow at time $t^* = 0.75$ and $R = 9500$. Length of the arrow indicates the speed of the vortex element. The values for the numerical parameters are $\Delta t^* = 0.03$, $\xi_{max} = 0.25$ and $M = 20$. These values are the same for figures 2, 3 and 5–8.

concentration of vortex elements and is located close to the separation point. The flow being pushed backwards towards the front stagnation point by the main vortex is met by the flow moving towards the rear, resulting in a pair of oppositely rotating secondary vortices. This complex configuration of the wake is referred to by Bouard & Coutanceau (1980) as the β-phenomenon. This pair of vortices was also observed by Prandtl & Tietjens (1957, page 292, plate 14, figure 33) and Ta Phuoc Loc & Bouard (1985), but neither Lecointe & Piquet (1984) nor Thoman & Szewczyk (1969) found evidence of this phenomenon in their numerical calculations. Note that in figures 3 and 4, the recirculating structure has its own centre of recirculation. This centre of recirculation is present in the photographs of Bouard & Coutanceau (1980) at $t^* = 1.00$ but is not present in either the photographs or the numerical results of Ta Phuoc Loc & Bouard (1985). Velocity vector fields and streamlines of subsequent development of the flow are presented in figures 5–8 corresponding to times $t^* = 1.25$, 1.5, 1.75 and 2.00 respectively.

When the Reynolds number is changed slightly, from $R = 9500$ to 10^4, the flow development remains nearly the same, but when the Reynolds number is changed to $R = 3000$ there is a drastic alteration in the development of the flow. At time $t^* = 1.50$ (figure 9), the geometry of the wake consists of three vortices – a pair of oppositely rotating secondary vortices in the secondary vortex region and one in the rear of the cylinder. This configuration (see also figure 10 corresponding to $t^* = 2.25$), referred to as the α-phenomenon, was observed by Bouard & Coutanceau (1980) experimentally and Lecointe & Piquet (1984) and Ta Phuoc Loc & Bouard (1985) numerically at $R = 3000$, and by Rogers *et al.* (1985) numerically and Nagata *et al.* (1985*a*) experimentally at $R = 1000$.

4.3. *Flows at other numerical parameters*

Previous work by Sethian & Ghoneim (1986) has shown the numerical convergence of the hybrid random vortex method. Their detailed and exhaustive analysis applied the random-vortex method to viscous, two-dimensional incompressible flow, comparing results from physical experiments with computed solutions obtained after

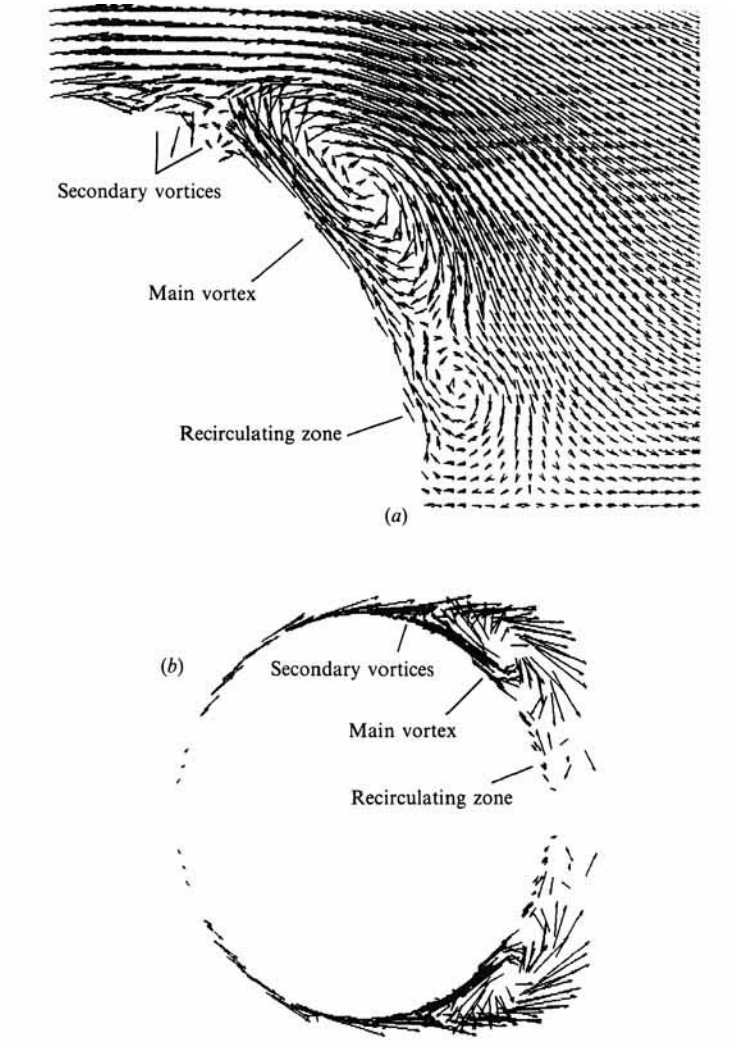

FIGURE 3. Flow past a cylinder at $t^* = 1.00$ and $R = 9500$. (*a*) Plot of the velocity vector field. (*b*) Plot of the velocity of each vortex element in the flow at that time. (*c*) Plot of the streamlines in the wake of the cylinder above the x-axis. The flow is symmetric.

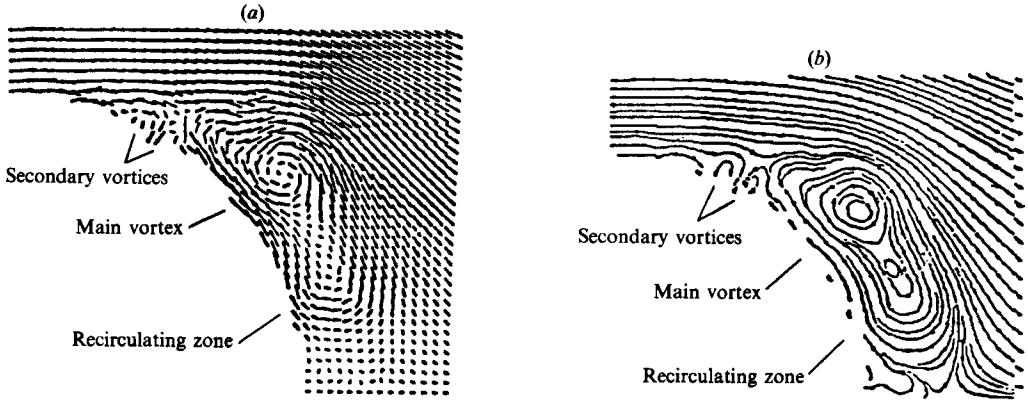

FIGURE 4. (*a*) The velocity vector field and (*b*) the streamline pattern for flow at $R = 10^4$ and time $t^* = 1.00$. This solution was generated by simulating the inviscid equations in the outer region and the viscous equations in the boundary layer. The values of the numerical parameters are $\Delta t^* = 0.05$, $\xi_{\max} = 0.50$ and $M = 20$.

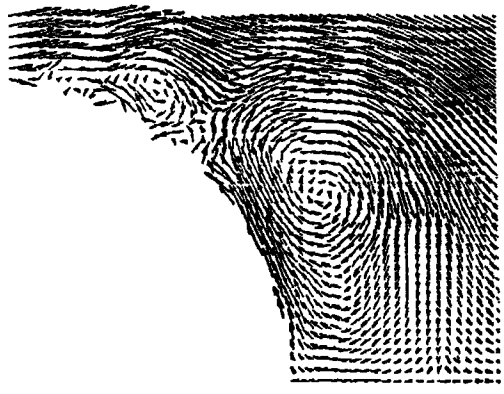

FIGURE 5. Velocity vector field at time $t^* = 1.25$ and $R = 9500$.

variation of choice of time step, number of particles, boundary-layer resolution, core size and size of the domain. Their results for unsteady high-Reynolds-number flow indicate that an increased number of vortices will provide better resolution provided the time step is suitably decreased so that the advection error remains small in comparison with the physical diffusion scale. For further details and discussion on the numerical convergence of the method, please see Sethian & Ghoneim (1986).

In the present paper, numerical experiments are performed using (i) different Reynolds numbers, (ii) different set of random numbers to model the diffusion equation, (iii) different time step, (iv) different maximum values for $\xi_{\max}$, (v) different values for h and (vi) first- and second-order approximations for the velocities u, v. Results indicate that the numerical method is appropriately sensitive to changes in R. Moreover, the structures in the flow do not change noticeably so long as the random numbers used are sampled from a Gaussian distribution of mean zero and variance $2\Delta t/R$. Refining other numerical parameters such as changing Δt^* from 0.03 to 0.02, the value for $\xi_{\max}$ from 0.25 to 0.2 and the value for M from 20 to 30,

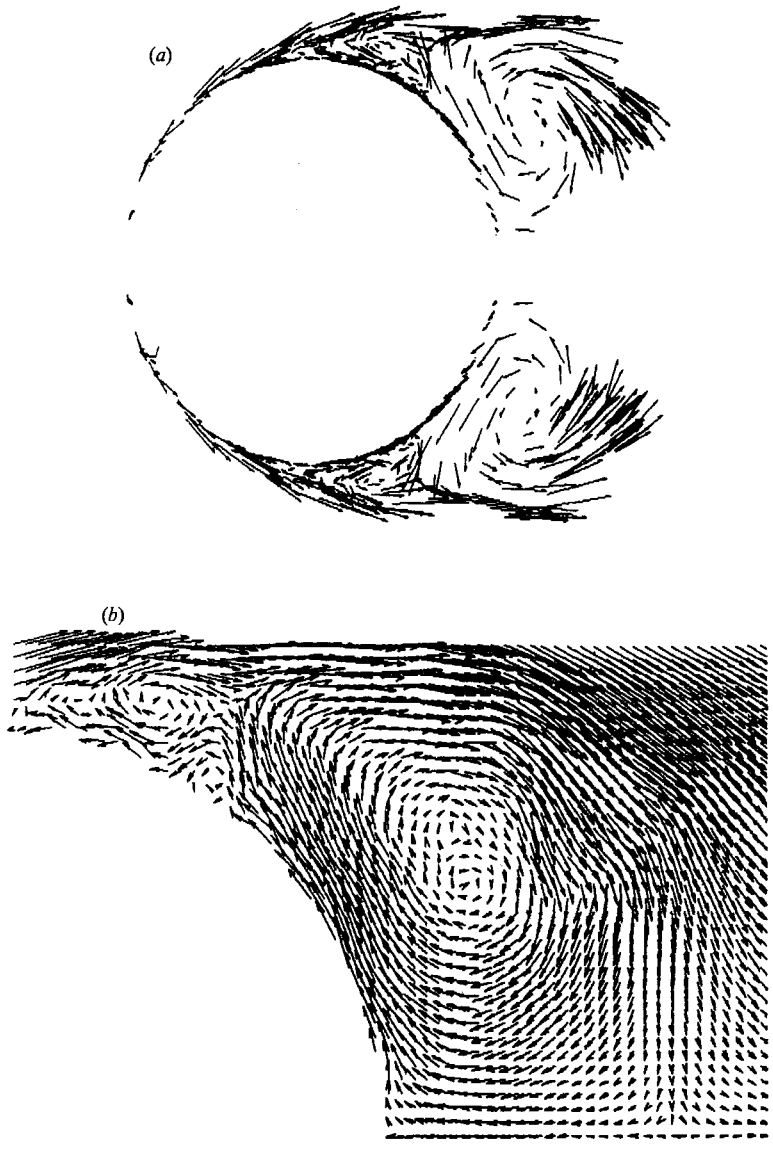

FIGURE 6. (*a*) Plot of the induced velocity of each vortex element in the flow at time $t^* = 1.50$ and $R = 9500$. (*b*) Corresponding velocity vector field.

does not produce significant improvements in the solution presented nor does it alter the solution in any physically meaningful way. For the above-specified values of the parameters, what variability that exists in the solutions appears in the numerical functionals which vary slightly from one computer run to another. When runs using one set of values are averaged and compared to runs using refined values the difference is small. The general structures and the general development of the flow in the initial unsteady stages as described in this paper (i.e. the α-phenomenon) are not destroyed even with large time steps and $\xi_{\max}$. Changing and refining numerical parameters may have a greater effect on the solution after a longer period of time or on the steady solution. Since our simulation is for the initial unsteady stages of

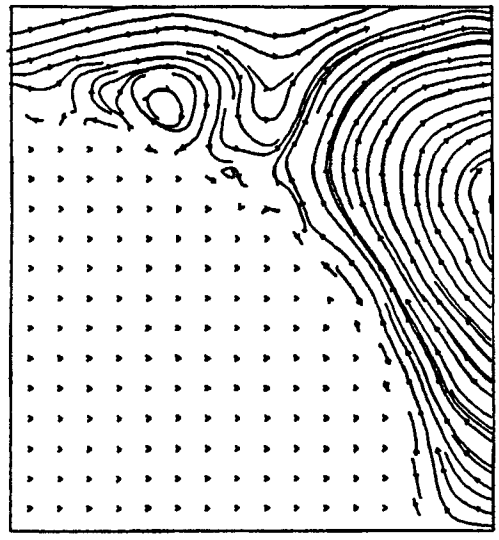

FIGURE 7. Detailed streamline pattern of the secondary vortex region for flow at $R = 9500$ at time $t^* = 1.75$.

development, and not the steady solution, the higher-order-accurate approximation for the velocity of the sheets produces better results. (Detailed plots for the above numerical experiments have been done but are not included because of their similarity to results already presented in this paper.) To obtain more accurate solutions the method will need to be revised to give higher-order accuracy in the approximations throughout, and a new approach will need to be developed to deal with the coupling in the method.

Calculations are also performed for the cases where the equations simulated were (i) inviscid in the outer flow and viscous in the boundary layer, and (ii) the parabolized Navier–Stokes equations. The solution for the inviscid–viscous interaction of the Euler and boundary-layer equations gives results that are better than the case where the parabolized Navier–Stokes equations are used (see figure 4).

4.4. *Other numerical functionals*

4.4.1. *Velocity on the wake axis*

The u-velocity on the x-axis behind the cylinder is plotted in figures 11 and 12 for $R = 9500$ and 3000 respectively. The portion of the curve that is positive corresponds to the positive u-velocity and the negative portion is backflow on the wake axis. Note that the rear stagnation point is situated at point (1.0, 0.0) and the diameter of the cylinder is 2.

It should be noted that the difference in the graphs (between our calculations and those of Bouard & Coutanceau 1980 and Ta Phuoc Loc & Bouard 1985) can be caused by one vortex element having a large random walk in the downstream direction. Since the random-walk component of the flow is drawn from a Gaussian distribution of mean zero and variance $2\Delta t/R$, a small percentage of the elements can have a large random-walk component. For the case $R = 3000$, the velocity on the wake axis is not as great as indicated by Ta Phuoc Loc & Bouard (1985) or Bouard & Coutanceau (1980) at latter times. It is difficult to make meaningful comparisons of these results

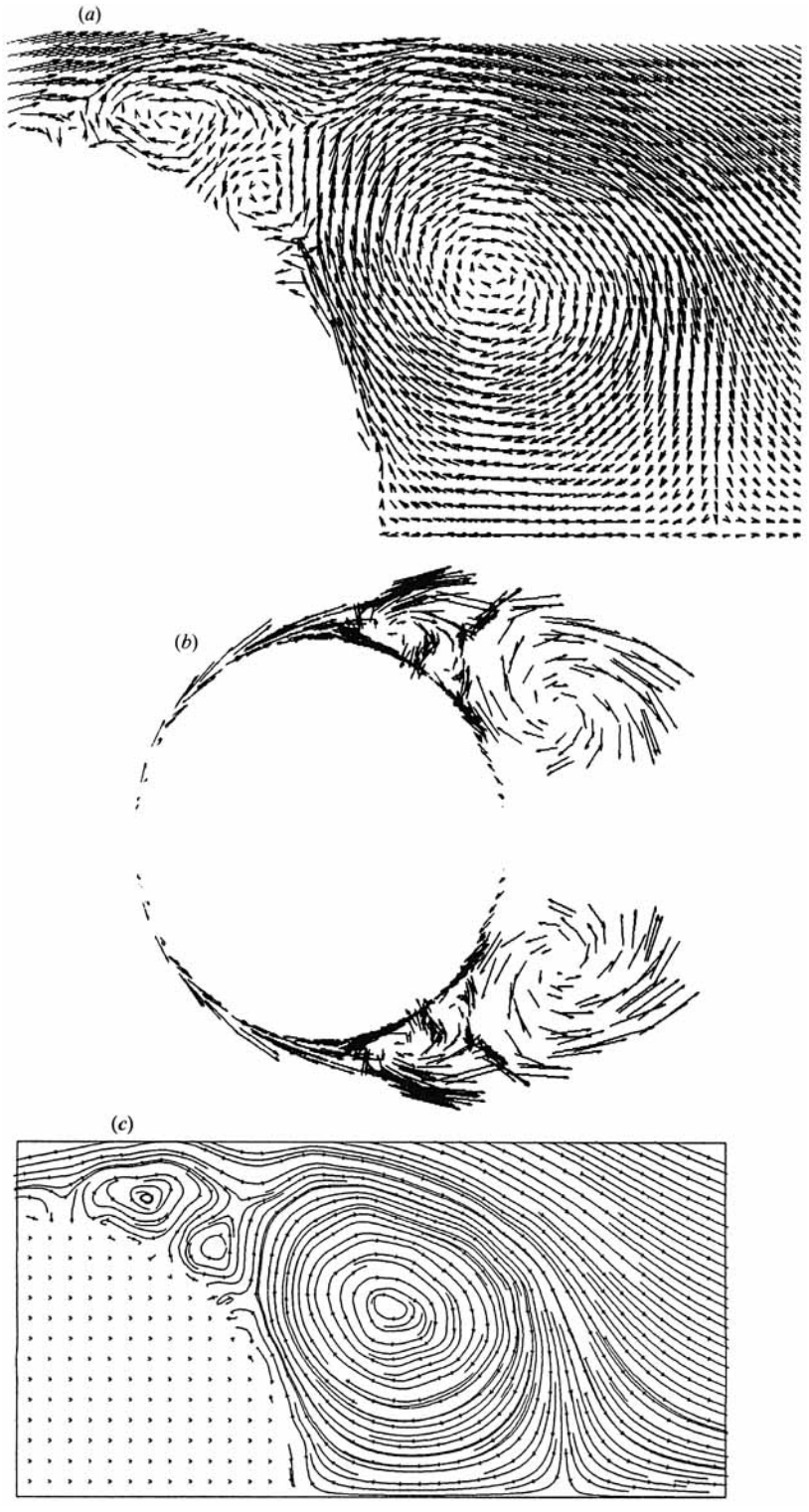

FIGURE 8. Flow past a cylinder at $t^* = 2.00$ and $R = 9500$. (*a*) Plot of the velocity vector field. (*b*) Plot of the velocity of each vortex element in the flow. (*c*) Plot of the streamlines in the wake of the cylinder above the x-axis. The flow is symmetric.

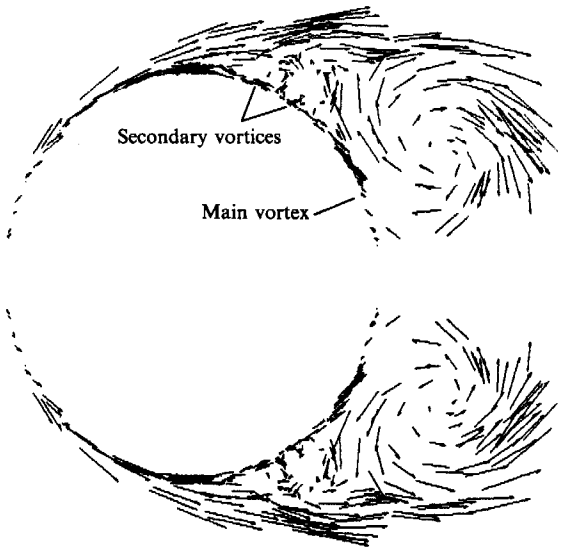

FIGURE 9. Plot of the induced velocity of each vortex element in the flow at time $t^* = 1.50$ and $R = 3000$.

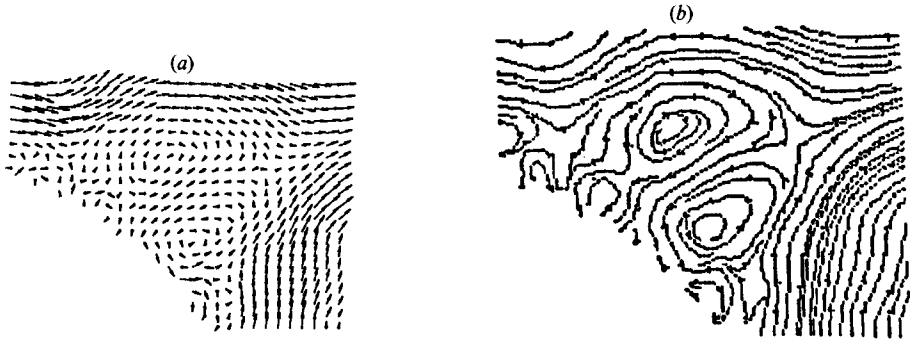

FIGURE 10. (*a*) Detailed velocity vector field and (*b*) streamline pattern of the secondary vortex region for flow at $R = 3000$ at time $t^* = 2.25$.

since no error bars or statistical analysis were given in the published experimental data.

4.4.2. *Drift of the core and length of the wake*

The curves L/D, a/D and $b/2D$ are plotted in figures 13 and 14 for $R = 10^4$, 9500 and 3000. L/D measures the length of the recirculating zone; L is the distance between the rear stagnation point and the point where the $-u_{\max}/U_\infty$ curves in figures 11 and 12 cross the wake axis. $(a/D, b/D)$ are the coordinates of the core of the main vortex measured from the rear stagnation point and normalized by the diameter. The curves a/D and $b/2D$ measure the drift of the core of the main vortex (see figure 1 for reference).

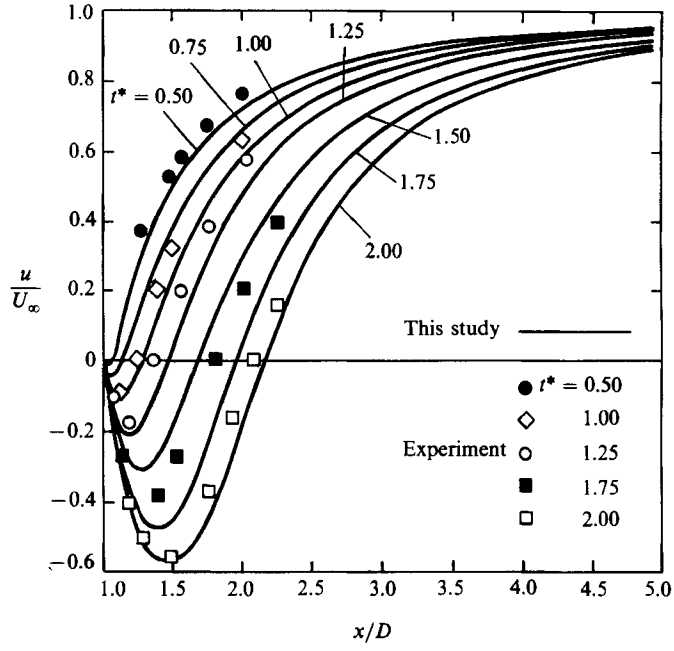

FIGURE 11. Velocity on the wake axis, $R = 9500$.

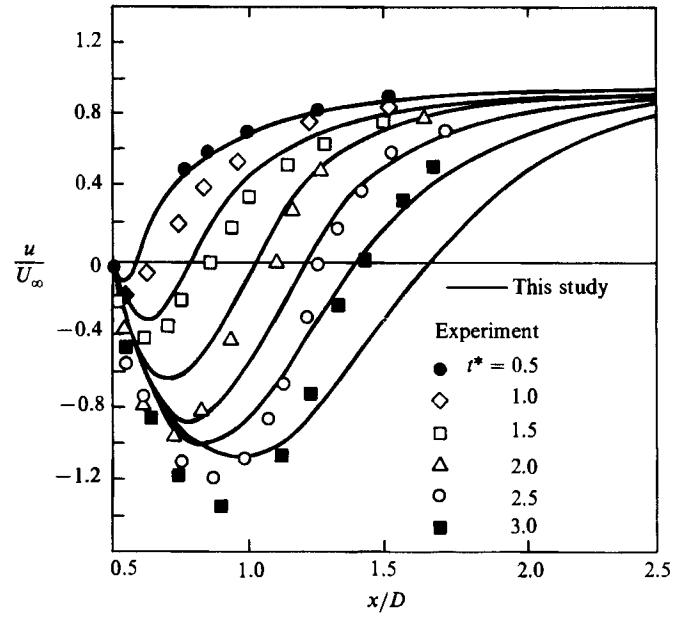

FIGURE 12. Velocity on the wake axis, $R = 3000$.

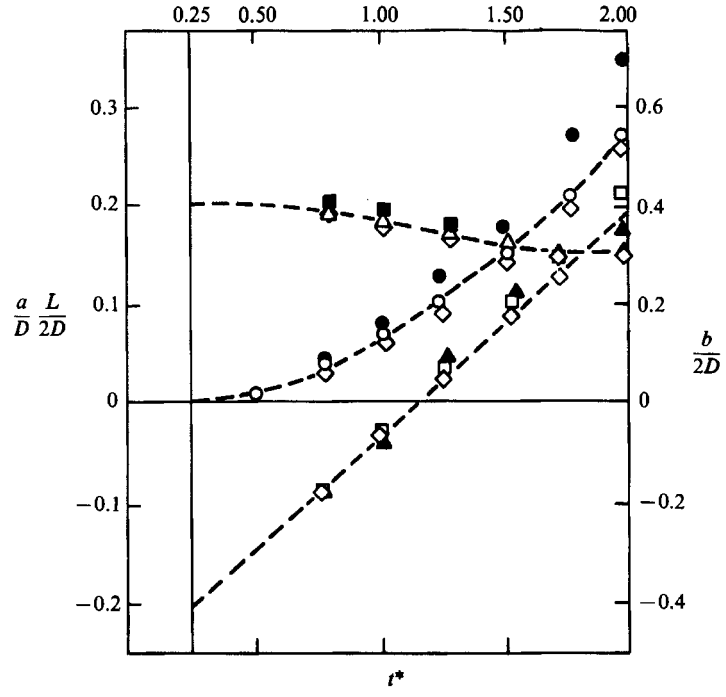

FIGURE 13. The length of the recirculating zone, L/D; and the drift of the core of the main vortex, a/D, $b/2D$.

	a/D	$b/2D$	$L/2D$
$R = 10^4$, $M = 20$, $\Delta t^* = 0.05$, $\xi_{max} = 0.50$	□	■	●
$R = 9500$, $M = 20$, $\Delta t^* = 0.03$, $\xi_{max} = 0.25$	▲	△	○
$R = 9500$ (experimental results of Bouard & Coutanceau 1980)	◇	◇	◇

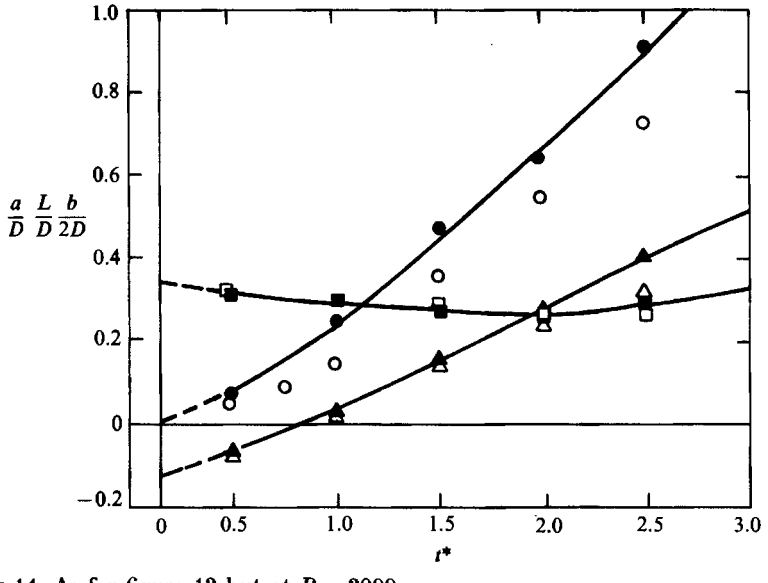

FIGURE 14. As for figure 13 but at $R = 3000$.

	a/D	$b/2D$	$L/2D$
This study	—▲—	—■—	—●—
Experimental results of Bouard & Coutanceau (1980)	△	□	○

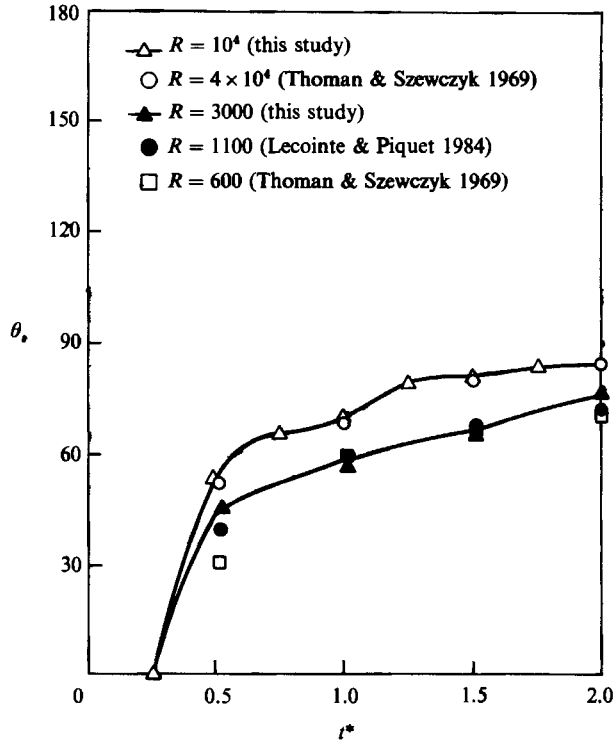

FIGURE 15. Transient separation point.

4.4.3. *Angle of separation*

Assuming that the point of separation is where the streamlines leave the body, we are able to calculate the angle of separation at regular intervals of the flow development. These data points are connected in figure 15 by a cubic spline. For $R = 3000$, a cubic-spline interpolation with smoothing is used. This graph shows satisfactory agreement with other experimental and numerical results.

5. Conclusion

A grid-free hybrid random vortex numerical method is used to study the unsteady flow development behind an impulsively started circular cylinder. At Reynolds numbers 9500 and 10^4, the flow development is very rapid and complex. By tracking the creation, diffusion and convection of vorticity, we are able to distinguish between the vortex structures and the areas of recirculation in the wake. Knowing the distribution of vorticity (vortex elements) allows us to predict which structures in the flow will grow and which ones will disappear. Our solution gives insight into the mechanism that controls the development of the complex structures in the wake at high Reynolds numbers. The results of our simulations also indicate that our numerical method is appropriately sensitive to changes in the Reynolds number R; changing R by a small amount does not alter the development of the flow significantly, but changing R by a large amount (to 3000) completely alters the development of the flow. The flow development at these Reynolds numbers corresponds well with known experimental and numerical results. The success of our

simulation lies in the ability of the method to accurately track the creation, diffusion and convection of vortex elements. The storage and computational time requirement is small compared with that needed to solve the same problem by a fourth-order-accurate finite-difference method on a 101×301 grid.

REFERENCES

ANDERSON, C. & GREENGARD, C. 1985 On vortex methods. *SIAM J. Numer. Anal.* **22**, 413–440.

AREF, H. 1983 Integrable, chaotic and turbulent vortex motion in two-dimensional flows. *Ann. Rev. Fluid Mech.* **15**, 345.

BATCHELOR, G. K. 1967 *An Introduction to Fluid Dynamics*. Cambridge University Press.

BEALE, J. T. & MAJDA, A. 1981 Rates of convergence for viscous splitting of the Navier–Stokes equations. *Maths Comp.* **37**, 243.

BEALE, J. T. & MAJDA, A. 1982*a* Vortex methods I: convergence in three dimensions. *Maths Comp.* **39**, 1.

BEALE, J. T. & MAJDA, A. 1982*b* Vortex methods II: higher order accuracy in two and three dimensions. *Maths Comp.* **39**, 28.

BOUARD, R. & COUTANCEAU, M. 1980 The early stage of development of the wake behind an impulsively started cylinder for $40 < Re < 10^4$. *J. Fluid Mech.* **101**, 583.

CHEER, A. Y. 1978 *Program BOUNDL*, LBL-6443, *Sup. Rep.*, Lawrence Berkeley Laboratory, University of California, Berkeley.

CHEER, A. Y. 1983*a* Numerical study of incompressible slightly viscous flow past blunt bodies and airfoils. *SIAM J. Sci. Stat. Comput.* **4**, 685.

CHEER, A. Y. 1983*b* Numerical analysis of time dependent flow structures generated by an impulsively started circular cylinder in a slightly viscous incompressible fluid. *Center for Pure and Applied Mathematics, Rep.* PAM-145. University of California, Berkeley.

CHORIN, A. J. 1973 Numerical study of slightly viscous flow. *J. Fluid Mech.* **57**, 785.

CHORIN, A. J. 1978 Vortex sheet approximation of boundary layers. *J. Comp. Phys.* **27**, 428.

CHORIN, A. J. 1980 Vortex models and boundary layer instability. *SIAM J. Sci. Stat. Comput.* **1**, 1.

COUTANCEAU, M. & BOUARD, R. 1977 Experimental determination of the main features of the viscous flow in the wake of a circular cylinder in uniform translation. Part 2. Unsteady flow. *J. Fluid Mech.* **79**, 257.

COUTANCEAU, M. & BOUARD, R. 1979 Sur la formation de tourbillons 'secondaries' dans le sillage d'un cylindre soumis à un de part impulsif. *C. r. hebd. Se'ance. Acad Sci.* **288 B**, 45.

DENNIS, S. C. R. & STANIFORTH, A. N. 1971 A numerical method for calculating the initial flow past a cylinder in a viscous fluid. In *Proc. 2nd Intl Conf. on Numerical Methods in Fluid Dynamics* (ed. M. Holt). Lecture Notes in Physics, vol. 8, p. 343. Springer.

GHONEIM, A. F. & SHERMAN, F. S. 1985 Grid-free simulation of diffusion using random walk methods. *J. Comp. Physics* **61**, 1–37.

GOODMAN, J. 1987 Convergence of the random vortex method. *Comm. Pure Appl. Maths* **40**, 189.

GOTTLIEB, D. & ORSZAG, S. 1977 Numerical analysis of spectral methods: theory and applications. *CBMS-NSF Regional Conference series in Applied Mathematics* 26. SIAM.

HALD, O. H. 1979 Convergence of vortex methods for Euler equations: II. *SIAM J. Numer. Anal.* **16**, 726.

HALD, O. H. 1985 Convergence of vortex methods for Euler equations: III. *Center for Pure and Applied Mathematics, U C Berkeley, PAM*-270.

HALD, O. H. & DEL PRETE, V. M. 1978 Convergence of vortex methods for Euler equations. *Maths Comp.* **32**, 791.

HONJI, H. & TENEDA, S. 1969 Unsteady flow past a circular cylinder. *J. Phys. Soc. Japan* **27**, 1668.

INGHAM, D. B. 1968 Note on the numerical solution for unsteady viscous flow past a circular cylinder. *J. Fluid Mech.* **31**, 815.

LECOINTE, Y. & PIQUET, J. 1984 On the use of several compact methods for the study of unsteady incompressible viscous flow round a circular cylinder. *Computers Fluids* **12**, 255.

LEONARD, A. 1980 Vortex methods for flow simulation. *J. Comput. Phys.* **37**, 289.

LIN, C. L., PEPPER, D. W. & LEE, S. C. 1975 Numerical methods for separated flow solutions around a circular cylinder. *AIAA 2nd Computational Fluid Dynamics Conference, Hartford, Conn., June 10–20.*

MARCHIORO, C. & PULVIRENTI, M. 1982 Hydrodynamics in two dimension and vortex theory. *Commun. Math. Phys.* **84**, 483.

NAGATA, H., FUNADA, H., KAWAI, K. & MATSUI, T. 1985*a* Unsteady flows in the vortex region behind a circular cylinder started impulsively. *Bull. JSME* **28**, 2599.

NAGATA, H., FUNADA, H. & MATSUI, T. 1985*b* Unsteady flows in the vortex region behind a circular cylinder started impulsively. *Bull. JSME* **28**, 2608.

PAYNE, R. B. 1958 Calculations of unsteady viscous flow past a circular cylinder. *J. Fluid Mech.* **4**, 81.

PEYRET, R. & TAYLOR, T. D. 1983 *Computational Methods for Fluid Flow*. Springer.

PRANDTL, L. & TIETJENS, O. G. 1957 *Applied Hydro and Aeromechanics*. Dover.

PUCKETT, E. G. 1987 A study of the vortex sheet method and its rate of convergence. *Center for Pure and Applied Mathematics, U C Berkeley, PAM*-369.

ROBERTS, S. 1983 Accuracy of the random vortex method for a problem with non-smooth initial conditions. *Center for Pure and Applied Mathematics, U C Berkeley, PAM*-162.

ROGERS, S. E., KWAK, D. & KUAL, U. 1985 On the accuracy of the pseudocompressibility method in solving the incompressible Navier–Stokes equations. *AIAA 18th Fluid Dynamics and Plasmadynamics and Laser Conference, July 16–18, 1985, AIAA*-85-1689.

SETHIAN, J. A. & GHONIEM, A. F. 1986 Validation study of vortex methods. *Center for Pure and Applied Mathematics, UC Berkeley, PAM*-325.

SHEN, S. F. 1977 Finite-element methods in fluid mechanics. *Ann. Rev. Fluid Mech.* **9**, 421.

SON, J. S. & HANRATTY, T. J. 1969 Numerical solution for the flow around a cylinder at Reynolds numbers 40, 200 and 500. *J. Fluid Mech.* **35**, 369.

TA PHUOC LOC 1980 Numerical analysis of unsteady secondary vortices generated by an impulsively started circular cylinder. *J. Fluid Mech.* **100**, 111.

TA PHUOC LOC & BOUARD, R. 1985 Numerical solution of the early stage of the unsteady viscous flow around a circular cylinder: a comparison with experimental visualization and measurements. *J. Fluid Mech.* **160**, 93.

TELIONIS, D. P. & TSAHALIS, A. TH. 1974 Unsteady laminar separation over impulsively moved cylinders. *Acta Astronautics* **1**, 1487.

THOMAN, D. C. & SZEWCZYK, A. A. 1969 Time-dependent viscous flow over a circular cylinder. *Phys. Fluids Suppl. II* **12**, 1176.

VAN DOMMELEN, L. L. & SHEN, S. F. 1982 The genesis of separation. In *Numerical and Physical Aspects of Aerodynamic Flows* (ed. T. Cebeci), pp. 293–367. Springer.